ACS APPLIED MATERIALS & INTERFACES

Research Article

www.acsami.org

Nanoporous Gold Disks Functionalized with Stabilized G-Quadruplex Moieties for Sensing Small Molecules

Suyan Qiu,[†,¶] Fusheng Zhao,[†] Oussama Zenasni,[†] Jingting Li,[†] and Wei-Chuan Shih*[,†,‡,§,⊥]

[†]Department of Electrical and Computer Engineering, [‡]Department of Biomedical Engineering, [§]Program of Materials Science and Engineering, and [⊥]Department of Chemistry, University of Houston, 4800 Calhoun Road, Houston, Texas 77204, United States

[¶]Institute for Quality & Safety and Standards of Agricultural Products Research, Jiangxi Academy of Agricultural Sciences, Nanchang, Jiangxi 330200, P. R. China

Supporting Information

ABSTRACT: We report label-free small molecule sensing on nanoporous gold disks functionalized with stabilized Guanine-quadruplex (G4) moieties using surface-enhanced Raman spectroscopy (SERS). By utilizing the unique G4 topological structure, target molecules can be selectively captured onto nanoporous gold (NPG) disk surfaces via $\pi-\pi$ stacking and electrostatic attractions. Together with high-density plasmonic "hot spots" of NPG disks, the captured molecules produce a remarkable SERS signal. Our strategy represents the first example of the detection of foreign molecules conjugated to nondouble helical DNA nanostructures using SERS while providing a new technique for studying the formation and evolution of G4 moieties. The molecular specificity of G4 is known to be controlled by its unit sequence. Without losing generality, we have selected $d(GGT)_7GG$ sequence for the sensing of malachite green (MG), a known carcinogen frequently abused illegally in aquaculture. The newly developed technique achieved a lowest detectable concentration at an impressive 50 pM, two orders of magnitude lower than the European Union (EU) regulatory requirement, with high specificity against potential interferents. To demonstrate the translational potential of this technology, we achieved a lowest detectable concentration of 5.0 nM, meeting the EU regulatory requirement, using a portable probe based detection system.

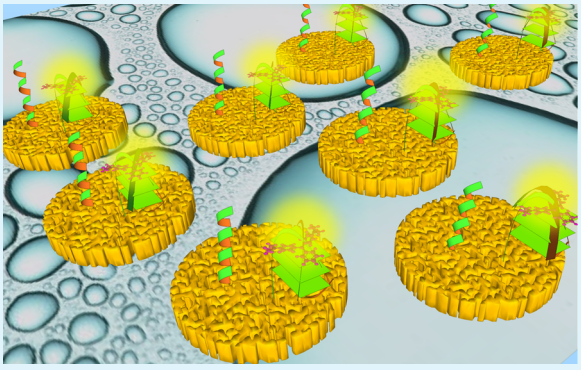

KEYWORDS: *G-quadruplex moieties, nanoporous gold disks, malachite green, surface enhanced Raman scattering, small molecule sensing*

1. INTRODUCTION

The formation of DNA topological structures[1] has been heavily studied for their pathogenesis implications[2] as well as their potential in highly specific molecular recognition in technologies such as microarray, polymerase chain reaction, and sequencing.[3,4] The formation and evolution of double-stranded DNA beta-helical nanostructures can be effectively reported by either prelabeled oligonucleotides or postlabeling using intercalating fluorescence dyes. Similarly, surface-enhanced Raman Scattering (SERS) has also been employed to report the Watson−Crick hybridization and melting of two complementary oligonucleotides.[5] In addition to unraveling the vast amount of genetic information in DNA molecules, DNA nanostructures serve as capture probes for the detection of conjugated small molecules when a sensitive reporting mechanism is available. For example, hairpin oligonucleotide has been a major design employed in molecular beacon probes. More recently, our group has developed hybridization-based microfluidic sensors with plasmon-enhanced fluorescence and SERS reporting mechanisms for cancer biomarker detection and quantification.[6,7] However, using label-free SERS for the detection of small molecules conjugated on DNA topological nanostructures other than double-stranded helix has never been demonstrated to date. Such technique not only provides novel label-free molecular sensing capabilities with high sensitivity and specificity, but also offers a novel tool for studying nondouble helical DNA nanostructures.

In this paper, we explore the potential of using Guanine-quadruplex (G4) topological structures as a capturing scaffold for the label-free sensing of small molecules, which at the same time report the conformation of the G4. G4s are readily formed by the $\pi-\pi$ stacking of two or more G-tetrads prevalent in guanine rich (G-rich) oligonucleotides. Such tetrameric structures consist of a planar arrangement of four guanine bases held together by a cyclic array of Hoogsteen hydrogen bonds. The central core of the G4 is negatively charged due to the orientation of the carbonyl group of each G-base toward the center of the G-tetrad.[8] Hence, several cations including Na^+,

Received: August 9, 2016
Accepted: September 13, 2016
Published: September 13, 2016

DOI: 10.1021/acsami.6b09767
ACS Appl. Mater. Interfaces 2016, 8, 29968−29976

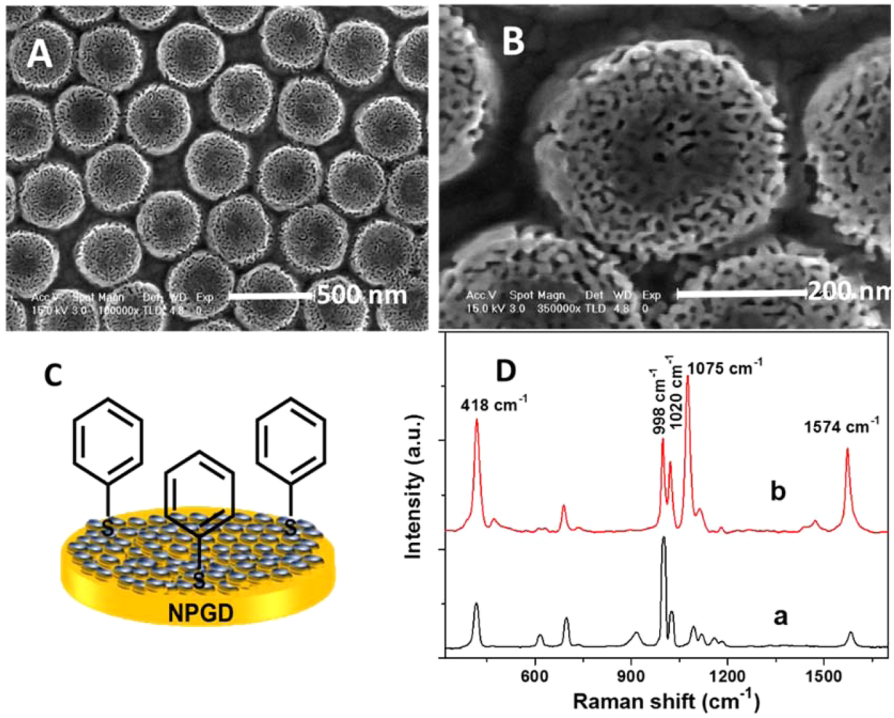

Figure 1. (A) SEM image of NPG disks after dealloyed for 30 s in 70% nitric acid; (B) SEM image of the corresponding single disk; (C) diagram of BT modified NPG disk; (D) (a) normal Raman spectra of BT and (b) SERS spectra of BT.

K^+, Pb^{2+}, and small cationic organic molecules are favored to conjugate with the G4 structure.[9−11] It is suggested that G4 moieties could be used as a capture scaffold for specific small molecules by varying its loop size and conformation such as parallel, antiparallel, and hybrid conformations.[12,13] For example, *N*-methyl mesoporphyrin IX (NMM) is known to conjugate to parallel G4 that is formed by the GGG TGG GTA GGG TGG G sequence, crystal violet (CV) to antiparallel G4 that is formed by the GGG TTA GGG TTA GGG TTA GGG sequence, and malachite green (MG) to the $d(GGT)_{13}G$ sequence. Therefore, highly specific small molecule sensors might be envisioned on custom-designed G4 nanostructures. Bhasikuttan et al. have elucidated the effectiveness of conjugating MG to G4 using a fluorescence technique.[14] This specific interaction has not been observed on single/double-stranded DNA and thus provides an effective means for the identification of G4 formation. However, this specific G4−MG conjugation has neither been studied using SERS, nor has SERS been demonstrated to be an effective monitoring technique for G4 conformation. Compared to the traditional fluorescence technique, the captured MG molecules would provide remarkable fingerprint peaks by SERS rather than one broad peak, which further advocates for the high specificity and sensitivity of the latter method.

Without losing generality, we select $d(GGT)_7GG$ sequence as an example to demonstrate sensitive and specific SERS detection of malachite green (MG), a well-known triphenylmethane dye with good antibacterial, antifungal, and antiparasitic properties.[15,16] MG is commonly employed as an active ingredient in veterinary drugs to resist fungal and parasitic infections in aquaculture due to its low cost and availability.[17,18] However, many countries ban or restrict the use of MG in fish farming due to its potential carcinogenic and mutagenic properties.[19] Despite its potential threat to human health, hundreds of cases of illegal use of MG have been reported by the European Union's (EU) Rapid Alert System for Food and Feed (RASFF) from 2003 to the present.[20] Therefore, the EU has mandated a sensor detection limit of 2 parts per billion (ppb) (~5.48 nM) for total MG and its reduced leuco-form. In addition, the U.S. Food and Drug Administration (FDA) prohibits the use of MG in aquaculture. Therefore, a more robust and reliable analytical technique is needed for a thorough and effective detection of MG residues in aquaculture products.

SERS can boost the sensitivity of Raman scattering to a molecular level, and it has been demonstrated as a powerful analytical tool for many analytes.[21−23] The enhanced Raman scattering primarily originates from localized field enhancement around nanostructures of a noble metal, such as gold and silver, and highly depends on the size, shape, composition, and assembly of those nanostructures.[24,25] A critical advantage of a SERS sensor lies in its potential for a label-free detection, which can profoundly impact molecular imaging and sensor technologies. To materialize these advantages, several SERS substrates have been designed to detect MG.[26] For example, Huang and co-workers used graphene oxide/gold nanocomposites as substrates to enhance the signal of MG through electrostatic interactions and $\pi-\pi$ stacking conjugation.[27] They demonstrated a lowest detectable concentration of 2.5 μM, which is three orders of magnitude above the EU regulation. Guo and co-workers designed a large-scale three-dimensional TiO_2 nanorod scaffold with decorated silver nanoparticles as a SERS substrate to identify MG with a detection limit of 1.0 pM. However, the specificity and the feasibility of such systems in real-world samples have not been tested.[28] Hence, it is our goal to develop a label-free SERS sensor with both high sensitivity and specificity for MG sensing.

Nanoporous gold (NPG) films have unique semirandom ligaments and porous channels that give rise to interesting gold nanostructures, which exhibit high surface-to-volume ratios.

DOI: 10.1021/acsami.6b09767
ACS Appl. Mater. Interfaces 2016, 8, 29968−29976

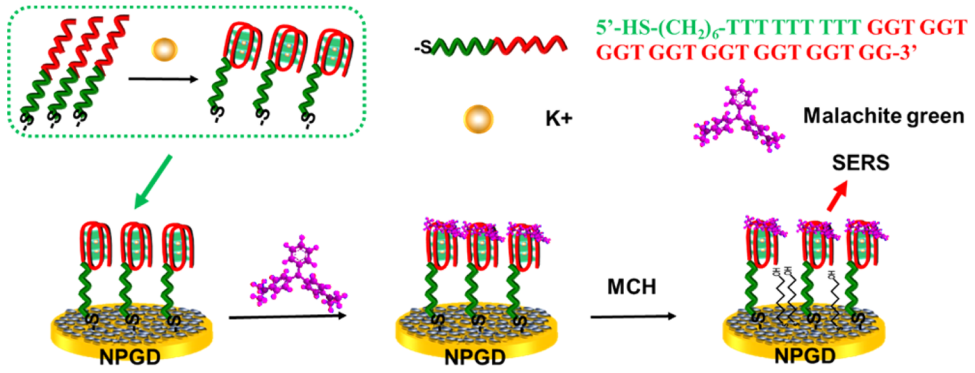

Figure 2. Schematic of G4 moieties-based SERS sensing platform.

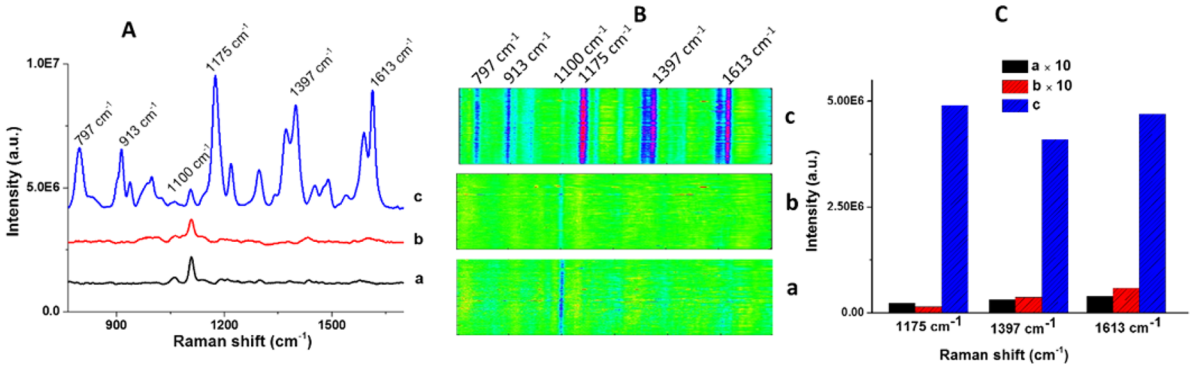

Figure 3. (A) SERS spectra and (B) image of different modified NPG disks; (a) MCH functionalized NPG disks immersed in MG solution (i.e., no G4); (b) G4-functionalized NPG disks immersed in buffer solution (i.e., no MG); (c) G4-functionalized NPG disks immersed in MG solution. (C) The corresponding SERS intensity from panel B at 1175 cm^{-1}, 1397 cm^{-1}, and 1613 cm^{-1}. The intensities from panels a and b were multiplied by 10 to be visible. The G4 concentration and MG concentration were 1.0 μM and 50 μM, respectively. Laser wavelength, 785 nm; power, 22.1 mW; lens, 60× objective; acquisition time, 10 s; accumulation time, 60 s.

Chen and co-workers have illuminated that the SERS intensity of polypyrrole was greatly enhanced on such NPG films.[29] However, the NPG in the form of semi-infinite thin films exhibits a weak plasmonic extinction and little tunability in the plasmon resonance frequency. To overcome these limitations, patterned NPG disks with subwavelength diameter and sub-100 nm thickness offer a large specific surface area and high-density sites of enhanced electric field, which together could greatly promote plasmon−molecule interactions.[30,31] A highly uniform SERS enhancement factor approaching 10^9 has been demonstrated on NPG disks.[32] Fundamentally, NPG disks provide a convenient "knob" for effective plasmonic engineering by varying the porous nanostructures, which has not been possible in others.[33,34] In addition, the surface modification protocol of NPG disks with a metal layer or a layer of nanoparticles can improve its plasmonic resonance. For example, small gold nanoparticles (AuNPs) that are loaded onto NPG disks can form additional hot-spots and further enhance the SERS performance. These results attest to NPG disks as a versatile class of high-performance SERS substrates.[35]

In this paper, we report the use of NPG disks functionalized with stabilized G4 moieties as a scaffold to capture MG molecules for label-free SERS sensing. The unique topological structure and loop size of G4 moieties can provide high specificity for binding to MG. However, the high-density hot-spots in NPG disks can contribute to the high sensitivity of the sensor. The novelty of this work is demonstrated in four aspects. First, this is the first example of SERS sensing of small molecules captured by nondouble-helical DNA nanostructures (e.g., G4). Second, the role that G4 plays in our approach differs from SERS sensing using aptamers, which are usually designed to capture large molecules such as proteins. Third, G4's capturing specificity with respect to small molecules has never been studied by SERS. Fourth, the sensing technique provides unprecedented sensitivity and specificity in real-world samples using a portable Raman system, which strongly advocates for potential field translation.

2. RESULTS AND DISCUSSION

2.1. Characteristics of the NPG Disks. The morphology of the NPG disks was investigated by scanning electron microscopy (SEM). As shown in Figure 1, panel A, the NPG disk structure with a diameter of 360 nm formed a semirandom array on the surface of a silicon wafer. The nanoporous network with pore sizes of ~15 nm can be observed in each individual disks, which offered a high surface-to-volume ratio for loading molecules (Figure 1B). These results are consistent with results in other published works by our group.[31,33]

To investigate the SERS performance of NPG disks, the enhancement factor (EF) was estimated using a benzenethiol (BT) self-assembled monolayer formed on the surface of NPG disks. In our study, NPG disks substrates were immersed in 1.0 mM BT solution for 30 min, followed by thorough rinsing with ethanol and deionized water to remove any excess of BT. Figure 1, panel D displays the average SERS spectrum from a single NPG disk. The EF was calculated from 1574 cm^{-1} to be 5.49×10^8 according to the eq 1:[36,37]

DOI: 10.1021/acsami.6b09767
ACS Appl. Mater. Interfaces 2016, 8, 29968−29976

$$EF = \frac{I_{SERS}}{I_{neat}} \times \frac{N_{neat}}{N_{SERS}} \quad (1)$$

Where I_{SERS} and I_{neat} represent the intensity of the SERS signal from a single disk and normal Raman signal, respectively. N_{SERS} and N_{neat} are the number of molecules that contributed to the SERS and normal Raman signals, respectively. Furthermore, the EF values at 1075 and 418 cm^{-1} were calculated to be 7.38×10^8 and 2.51×10^8, respectively. Details on the calculation of I_{SERS}, I_{neat}, N_{SERS}, and N_{neat} are presented in the Supporting Information.

2.2. Detection Mechanism for MG Molecules. The sensing scheme on NPG disks with functionalized G4 moieties is shown in Figure 2. Herein, the DNA sequence rich in G is selected to form G4 as the capturing scaffold. K^+ ions are used to stabilize the G4 moieties,[38] and 6-mercaptohexanol (MCH) is applied to block the nonspecific binding of small molecules.[39] Exposure of the G4-decorated NPG disks to MG molecules causes the electron-rich phenyl rings of MG to effectively bind on the face of the G4 moieties to form G4-MG conjugations through $\pi-\pi$ stacking; this conjugation renders rigidity to the planar structure of the MG molecule, thereby centering the charged MG molecule within G4. The electrostatic interaction between MG molecules and the G4 scaffold can further improve the stability of G4−MG conjugations.[14] A remarkable SERS signal can be observed from the captured MG molecules on the G4-functionalized NPG disks. In contrast, no SERS signal, except for that from MCH molecules, is detected in the absence of MG molecules due to the lack of MG molecules being captured by G4 moieties. As a result, a highly sensitive and specific SERS sensor can be developed to identify MG molecules.

2.3. Feasibility of the Label-Free SERS Sensing Platform. SERS data were collected after the steps depicted in Figure 2. As shown in Figure 3, panel A, only one significant SERS peak (about 1100 cm^{-1}) from MCH was detected in the absence of MG (Figure 3Ab). Similar results were obtained in the absence of G4 moieties (Figure 3Aa), which suggest that MG molecules could not be immobilized effectively onto the surface of NPG disks without G4 as the capturing scaffold as well as the effectiveness of MCH as a blocking-agent. Several SERS peaks are observed in the presence of MG molecules and G4 moieties (Figure 3Ac). Among these peaks, the conspicuous peaks at 1175 cm^{-1}, 1397 cm^{-1}, and 1613 cm^{-1} are assigned to the in-plane modes of C−H bending, *N*-phenyl stretching, and ring C−C stretching of MG molecules, respectively. The medium-intensity bands at 797 and 913 cm^{-1} are assigned to ring C−H out-of-plane bending.[40] The results suggest that MG molecules were captured by G4 moieties and assembled on the surface of NPG disks successfully. These results were further confirmed by examining their corresponding images (Figure 3B) collected by our line-scan Raman microscope (LSRM).[41,42] LSRM provides the capability of simultaneously monitoring 133 1-μm^2 spots, an essential capability for robust measurements and statistical analysis. In each image, the *x*-axis and *y*-axis correspond to the wavenumber and location, respectively. In other words, these images consist of 133 SERS spectra, each from a 1 μm^2 spot. Only a significantly single peak from MCH molecules was observed in the absence of MG or G4 moieties (Figure 3Ba,b) over the range of 760−1650 cm^{-1}, whereas several remarkable MG peaks appeared in the presence of MG (Figure 3Bc). Note that the MCH peaks do not overlap with any of the MG peaks, thereby providing unambiguous interpretation. The intensities at 1175 cm^{-1}, 1397 cm^{-1}, and 1613 cm^{-1} of G4 functionalized NPG disks with MG were much greater than that of without MG or G4 moieties (Figure 3C), which indicated that SERS signals from MCH molecules and G4 moieties would not interfere with MG detection.

To further confirm the interaction between G4 and MG molecules, the SERS spectra with and without G4 were examined. As can be seen from Figure S1, several salient peaks from MG molecules were observed in the absence of G4, which was caused by nonspecific binding of MG molecules. However, these peaks were near the noise level after incubation with the MCH solution (see inset in Figure S1), which suggest that the physisorbed MG molecules were replaced by MCH molecules through the strong binding affinity of the thiolated headgroup of MCH molecules. In contrast, the SERS intensity had no significant variation in the presence of G4 before and after incubating with the MCH solution, which indicated that the MCH molecules could not replace MG molecules that are captured by G4 moieties. In other words, the MG molecules were conjugated onto the surface of NPG disks through an interaction with G4 moieties rather than nonspecific binding on the surface of NPG disks, a key factor for high specificity.

X-ray photoelectron spectroscopy (XPS) was used to obtain compositional information on the surface of NPG disks after various modification steps including G4 functionalization, MCH blocking, and MG binding (Figure S2). In the S 2p region (Figure S2D), no significant peak was observed for the blank NPG disks (curve a in Figure S2D). On the other hand, two apparent peaks centered at 161.9 eV (S $2p_{3/2}$) and 163.0 eV (S $2p_{1/2}$) appeared after incubating NPG disks with G4 (curves b−d in Figure S2D), which are typical for sulfur bound to a gold surface[43] and confirm the immobilization of G4 moieties on the surface of NPG disks. In the C 1s regions (Figure S2B), the peak centered at 284.9 eV is attributed to the methylene carbons of the sugar group in the DNA sequence. The other peak centered at 286.9 eV is a result of C−N bonds, C−O bonds, and sugar−phosphate bonds of G4 moieties. In the N 1s region (Figure S2C), a broad peak, which consists of two peaks, was observed after NPG disks were functionalized with G4 moieties. Further, the peak centered at 399.3 eV is assigned to conjugated N−C bonds (sp^2; C═N−C), and the peak centered at 400.4 eV is designated to N−H bonds. To further examine changes after each modification step, the ratios of C 1s/Au 4f, N 1s/Au 4f, and S 2p/Au 4f were calculated to demonstrate the surface compositional variations at different modification stages, and the data are summarized in Table S1. The ratios of C 1s/Au 4f, N 1s/Au 4f, and S 2p/Au 4f significantly increased after the disks were immersed into the G4 solution (b in Table S1) when compared to the blank NPG disks (a in Table S1), which verified the successful assembly of G4 moieties on the surface of NPG disks through the specific Au−S bond. With the addition of the MCH solution, without MG molecules, the ratios of C 1s/Au 4f and S 2p/Au 4f increased as well, which is caused by the binding of MCH molecules. Meanwhile, the N 1s/Au 4f ratio slightly decreased in c (c in Table S1), which may be caused by the replacement of nonspecific bound G4 moieties by MCH molecules. Furthermore, in the presence of MG molecules, a further increase of the C 1s/Au 4f ratio was observed (d in Table S1), which is accompanied by no obvious increase of the N 1s/Au 4f and S 2p/Au 4f ratios when compared with that of without MG (c in Table S1). The reason might lie in the fact that MG molecules are mainly composed of carbon atoms and a very low

DOI: 10.1021/acsami.6b09767
ACS Appl. Mater. Interfaces 2016, 8, 29968−29976

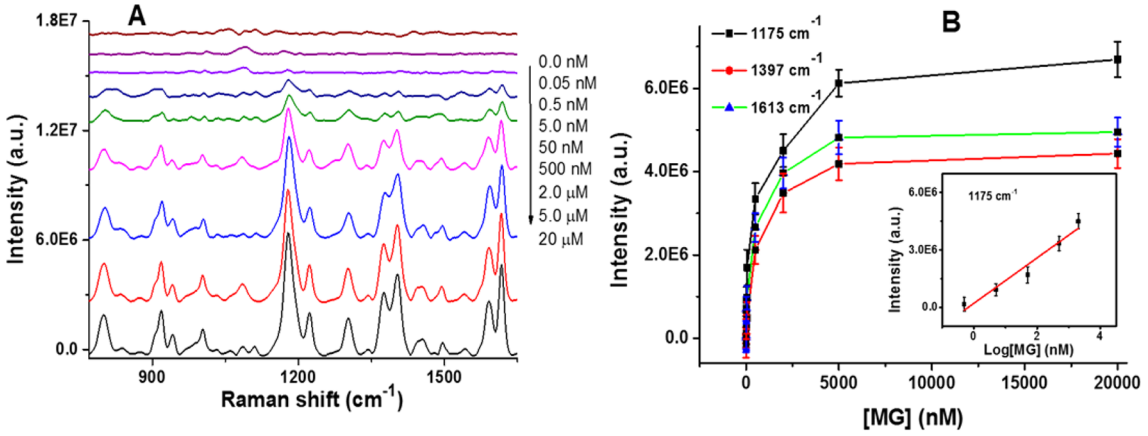

Figure 4. (A) SERS spectra from different MG concentrations; (B) SERS intensity at 1175 cm^{-1}, 1397 cm^{-1}, and 1613 cm^{-1} as a function of MG concentration. Inset shows a linear relationship between the SERS intensity at 1175 cm^{-1} and the logarithm of MG concentration at the range from 0.5−2000 nM. The laser wavelength was 785 nm with an acquisition time of 10 s with six accumulations. The error bars were calculated from at least three measurements on random spots on the same substrate.

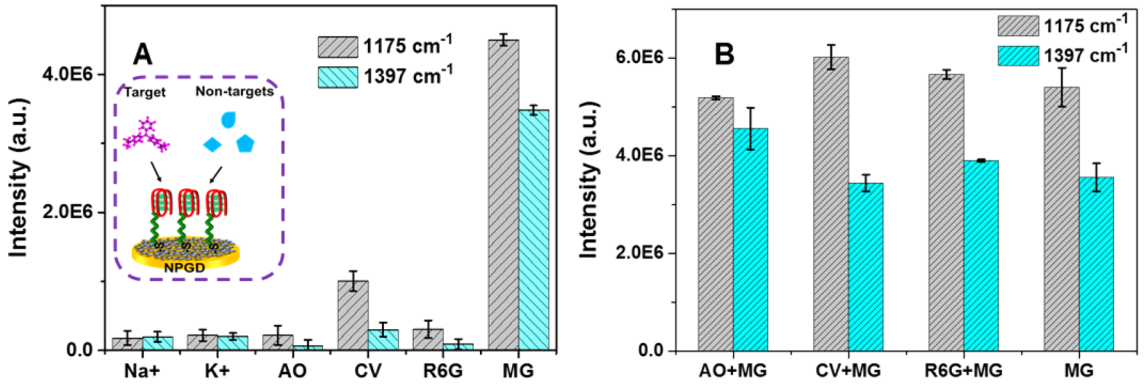

Figure 5. SERS intensities of (A) single interferents and (B) mixtures containing the individual interferents and MG at 1175 and 1397 cm^{-1}. Laser wavelength, 785 nm; lens, 60× objective; acquisition time, 10 s; accumulation time, 60 s. Concentrations of K^+ and Na^+ were 50 mM. Concentrations of AO, CV, R6G, and MG were 2.0 μM.

percentage of nitrogen atoms. These results provide an independent assessment of the surface composition throughout all the modification steps.

2.4. Effect of G4 Concentration on the SERS Sensor. The effect of G4 concentration was examined since it directly influences the surface density of capturing sites. The data summarized in Figure S3 revealed that the SERS intensity was enhanced sharply with increasing DNA concentration in the range of 100 pM to 100 nM due to an increase of capturing sites formed on the NPG disks. However, the intensity increase decreased and reached a plateau in the range from 100 nM to 1.00 μM. To achieve the best performance, 1.00 μM was used for all subsequent experiments. Additionally, a detectable SERS signal, with a signal-to-noise ratio larger than 3 (SNR > 3), was obtained in the presence of very low G4 concentration (100 pM). The results not only indicate that G4 moieties are highly effective in capturing MG molecules, but also suggest that this SERS sensing platform can be explored to report the formation of G4 moieties.

2.5. Sensitivity for MG Detection. To demonstrate the sensitivity of our technique, SERS measurements were obtained from a series of MG concentrations. In Figure 4, the SERS intensity increased with the MG concentration in the range of 50 pM to 5.0 μM; the intensity then reached a plateau after 5.0 μM, which suggests a slower binding event of MG molecules onto the surface of G4-functionalized NPG disks beyond 5.0 μM. Moreover, a good linear relationship between SERS intensity and the logarithm of MG concentration was observed in the range of 0.5−2000 nM. The prominent peak at 1175 cm^{-1} can be observed at 50 pM of MG, the best high-specificity lowest detectable concentration ever reported by SERS. Additionally, when compared to 50 nM of MG, an obvious sparsity of SERS image with 50 pM of MG was identified (Figure S4), a strong indication of single molecule detection.[44] The high sensitivity may be attributed to three factors: (1) the high enhancement of local electromagnetic fields from high-density hot-spots on NPG disks; (2) the high affinity of G4 moieties formed by the unique G-rich DNA to MG molecules; or (3) the nanoporous structure of NPG disks provides a high surface-to-volume ratio for loading more G4 moieties, thus capturing more MG molecules onto the surface of NPG disks.[45]

2.6. Specificity Study. To assess the specificity of our designed platform toward MG molecules, several common dyes and metal ions were examined. The test included 2.0 μM of acridine orange (AO), crystal violet (CV), rhodamine 6G (R6G), MG, and 50 mM Na^+ and K^+. Furthermore, we used the intensities of two SERS peaks at 1175 and 1397 cm^{-1} as points for comparison. Figure 5 shows that the SERS intensities of interferents, except for CV, are over an order of magnitude lower than that of the target MG molecules. On the other hand,

DOI: 10.1021/acsami.6b09767
ACS Appl. Mater. Interfaces 2016, 8, 29968−29976

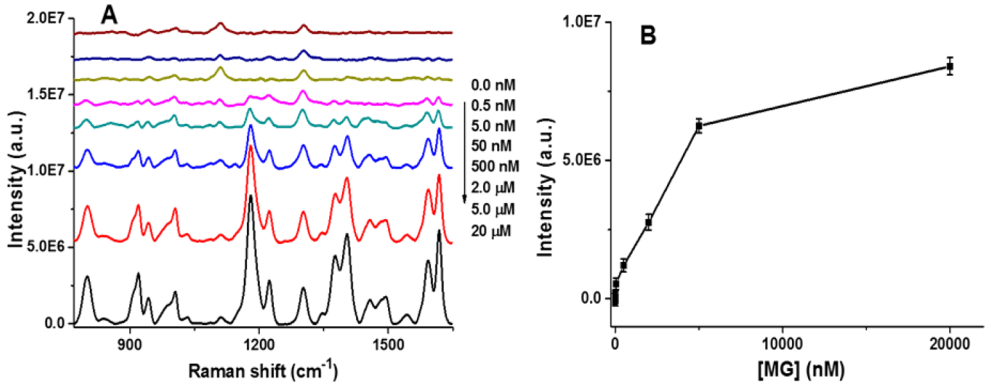

Figure 6. (A) SERS spectra in fish samples spiked with various MG concentrations; (B) the corresponding SERS intensity change at 1175 cm^{-1}. Laser wavelength, 785 nm; power, 22.1 mW; lens, 60× objective; acquisition time, 10 s; accumulation time, 60 s.

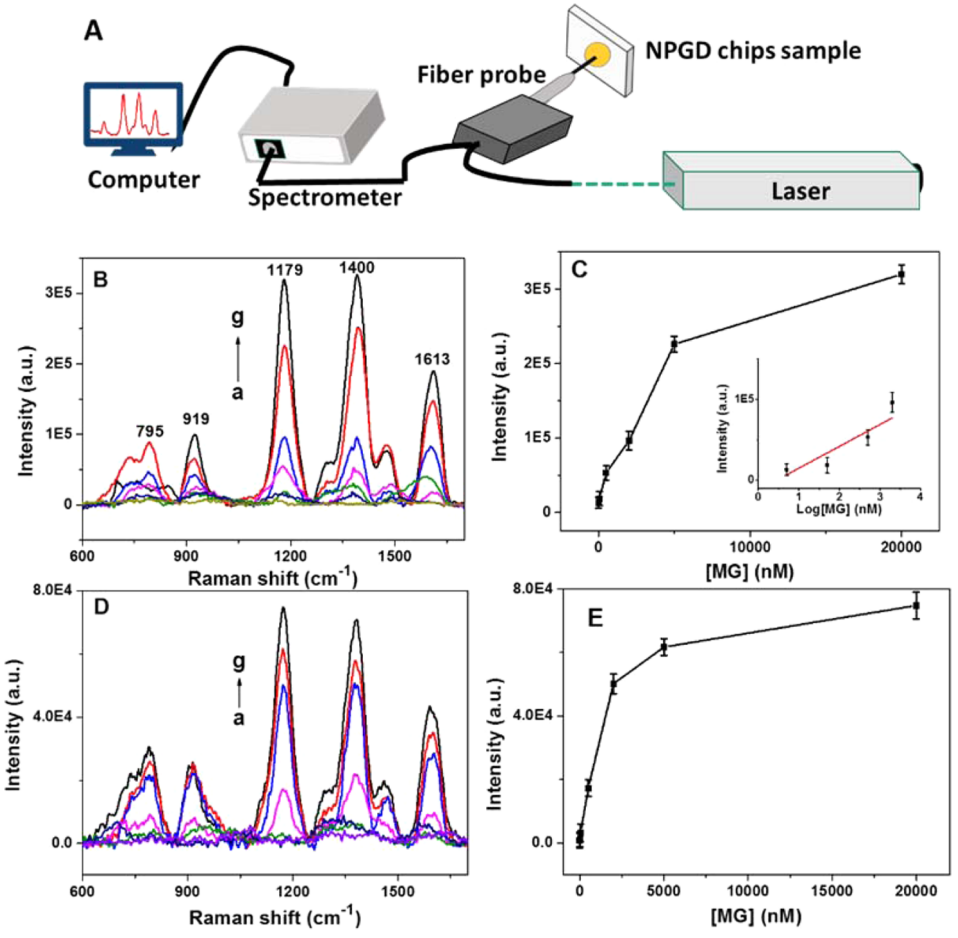

Figure 7. (A) Portable Raman system with an optical fiber probe; (B) SERS spectra of various MG concentrations in PBS buffer solution; from a−g are 0.0 nM, 5.0 nM, 50 nM, 500 nM, 2000 nM, 5.0 μM, and 20 μM, respectively; (C) plot of SERS intensity at 1179 cm^{-1} versus MG concentration, inset: linear range of SERS intensity at 1179 cm^{-1} versus MG concentration 5.0−2000 nM. (D) SERS spectra of fish samples spiked with various MG concentrations; from a−g are 0.0 nM, 5.0 nM, 50 nM, 500 nM, 2000 nM, 5.0 μM, and 20 μM, respectively; (E) Pplot of SERS intensity at 1179 cm^{-1} versus MG concentration. Laser wavelength, 785 nm; acquisition time, 0.5 s; accumulation time, 30 s.

CV, albeit having a molecular structure similar to MG, only produced about $\sim^1/_5$ of the peak height of MG at 1175 cm^{-1}, which suggests good specificity. Furthermore, we have also carried out experiments to investigate the potential competition between various coexisting dye molecules. As shown in Figure 5, panel B, the relative standard deviations (RSDs) of the intensities at 1175 and 1397 cm^{-1} were 6.45% and 10.08%, respectively, which further confirm the high specificity. The unique topological structure and loop size of G4 moieties has been shown to play a decisive role in the binding interaction,[46] which strongly favors MG. Therefore, the high specificity for MG detection by our technique is attributed to two salient features: (1) the SERS spectra provide the fingerprint for different species; (2) the G4 moieties show high efficiency for capturing MG molecules.

DOI: 10.1021/acsami.6b09767
ACS Appl. Mater. Interfaces 2016, 8, 29968−29976

2.7. Sensor Performance in Complex Samples. To further evaluate the translational value of our sensor in complex, real-world samples, fish meat spiked with MG, were employed as a model.[47] Zhong et al. used flexible AuNPs substrates to detect MG on the surface of fish that were immersed in MG contaminated aqueous medium. However, their lowest detection limit of MG in aqueous medium was 100 nM, which is two orders of magnitude higher than that of the European Union (EU) requirement (~5.48 nM). In our experiments, purchased fish were turned into a homogenate. Then the fish homogenate (2 g) mixed with 10 mL of PBS buffer solution was incubated at room temperature overnight. After that, the solution was filtered through a 0.22 μm membrane filter to remove the residue. Various MG concentrations were used to spike the resulting supernatant and measured using our sensor. As shown in Figure 6, the SERS intensity increased as MG concentration increased over the range of 500 pM to 5.00 μM and then increased slowly beyond 5.0 μM concentration. The trend is consistent with that obtained from using PBS buffer solution, which suggests that the sensor functions well in complex samples. Therefore, the proposed sensing system may be extended to other target assays in the biological and environmental fields while taking into account the possible need to modify the G4 sequence to accommodate for the target analyte.

2.8. Reproducibility. To evaluate the SERS performance of the proposed sensing platform, we explored its reproducibility on different NPG disks samples. The data summarized in Figure S5 represent five sensing experiments obtained from different NPG disks substrates. The RSDs of the intensities at 1175 cm^{-1}, 1397 cm^{-1}, and 1615 cm^{-1} were 3.76%, 5.77%, and 6.4%, respectively, which indicate good reproducibility for both MG detection and MG sensor preparation.

2.9. Sensor Performance Using a Portable Fiber Based Probe System. Although the above-mentioned SERS sensor exhibited excellent sensitivity and good specificity, a laboratory Raman system was employed. To demonstrate real time, on-site measurement in the field, a portable Raman system with an optical fiber probe was tested.[48−50] Figure 7, panel B displays the SERS signals with different MG concentrations that were collected in PBS buffer solutions using the fiber probe. The fiber probe gave results similar to the laboratory Raman system. In the absence of MG, no significant Raman peak was detected (curve a in Figure 7B). After incubation with MG, several Raman peaks at 795 cm^{-1}, 919 cm^{-1}, 1179 cm^{-1}, 1400 cm^{-1}, and 1613 cm^{-1} were detected, which were attributed to the captured MG molecules on the surface of the NPG disks. The peaks at 1179 cm^{-1}, 1400 cm^{-1}, and 1613 cm^{-1} appear as single peaks and not as double peaks that are detected by the LSRM system, which might be caused by the wider slit used in the fiber probe system. An increase in the MG concentration causes the SERS intensity to increase accordingly since more MG molecules are captured by G4 moieties on NPG disks. When MG molecules occupy all surface-bound G4 moieties, the SERS intensity reaches a plateau. A linear range was identified between the intensity and the logarithm of MG concentration from 5.0−2000 nM (inset in Figure 7C). The lowest detectable concentration was 5.0 nM, which suggests that this sensor can be employed with a portable Raman system. The difference between the linear relationships reported in Figure 4 and that in Figure 7 is due to the lower sensitivity of the portable Raman system compared to the line scan system.

To further examine the performance of the portable Raman system with respect to real-world samples, MG spiked fish solutions were also used as an example of a complex sample model. Results obtained were consistent with that in PBS buffer solutions (Figure 7D and 7E). The SERS intensity increased first and then reached a plateau beyond 5.0 μM. The lowest detected concentration was 5.0 nM, which meets the current EU regulatory requirements. These results demonstrate the feasibility of an on-site monitoring of MG for industrial and environmental applications.

3. CONCLUSIONS

In conclusion, a label-free SERS sensor for the detections of small molecules is first described using G4 moieties functionalized on NPG disks as a capturing scaffold. G4 is known to bind to various small molecules with high specificity when its sequence is properly designed. Herein, G4 moieties with $d(GGT)_7GG$ sequence are employed to capture MG molecules. The unique topological structure and loop size of G4 moieties provide good specificity, even in the presence of other common dyes, such as acridine orange, crystal violet, and rhodamine 6G, which further confirms the preferential binding of MG to G4 moieties. The impressive lowest detectable concentration at 50 pM, the lowest ever reported, has been achieved with good specificity. Furthermore, the sensor performance has been shown to meet the EU regulatory requirement by testing against real samples using a portable fiber probe, which suggests its high potential for field applications. Considering the emerging applications of MG molecules in biological fields, such as bacterial identification, site-specific inactivation of RNA transcripts, and intracellular Raman reporters, the presented SERS sensing system has the potential to be extended to other biological analysis and diagnoses. More importantly, the strategy provides a new path for the development of label-free SERS sensors using DNA topologically functionalized plasmonic nanostructures.

■ ASSOCIATED CONTENT

Supporting Information

The Supporting Information is available free of charge on the ACS Publications website at DOI: 10.1021/acsami.6b09767.

Methods; supporting figures and tables (PDF)

■ AUTHOR INFORMATION

Corresponding Author

*E-mail: wshih@central.uh.edu. Fax: +1-713-743-4444. Phone: +713-743-4000.

Author Contributions

S.Q. and W.-C.S. conceived the idea, designed the study, and wrote the paper. F.Z. prepared the NPG disks. O.Z. performed the XPS measurements. J.L. analyzed the Raman data.

Notes

The authors declare no competing financial interest.

■ ACKNOWLEDGMENTS

W.-C.S. acknowledges the National Science Foundation (NSF) CAREER Award CBET-1151154, NSF CBET-1605683, and a grant from the Gulf of Mexico Research Initiative (GoMRI-030).

DOI: 10.1021/acsami.6b09767
ACS Appl. Mater. Interfaces 2016, 8, 29968−29976

REFERENCES

(1) Murayama, Y.; Uhlmann, F. Biochemical Reconstitution of Topological DNA Binding by the Cohesin Ring. *Nature* **2014**, *505* (7483), 367−371.

(2) Murat, P.; Zhong, J.; Lekieffre, L.; Cowieson, N. P.; Clancy, J. L.; Preiss, T.; Balasubramanian, S.; Khanna, R.; Tellam, J. G-Quadruplexes Regulate Epstein-Barr Virus−Encoded Nuclear Antigen 1 Mrna Translation. *Nat. Chem. Biol.* **2014**, *10* (5), 358−364.

(3) Shin, Y. J.; Kumarasamy, V.; Camacho, D.; Sun, D. Involvement of G-Quadruplex Structures in Regulation of Human Ret Gene Expression by Small Molecules in Human Medullary Thyroid Carcinoma Tt Cells. *Oncogene* **2015**, *34* (10), 1292−1299.

(4) Zhou, B.; Liu, C.; Geng, Y.; Zhu, G. Topology of a G-Quadruplex DNA Formed by C9orf72 Hexanucleotide Repeats Associated with Als and Ftd. *Sci. Rep.* **2015**, *5*, 16673.

(5) Johnson, R. P.; Richardson, J. A.; Brown, T.; Bartlett, P. N. A Label-Free, Electrochemical Sers-Based Assay for Detection of DNA Hybridization and Discrimination of Mutations. *J. Am. Chem. Soc.* **2012**, *134* (34), 14099−14107.

(6) Qi, J.; Zeng, J.; Zhao, F.; Lin, S. H.; Raja, B.; Strych, U.; Willson, R. C.; Shih, W. C. Label-Free, in Situ Sers Monitoring of Individual DNA Hybridization in Microfluidics. *Nanoscale* **2014**, *6* (15), 8521−8526.

(7) Santos, G. M.; Zhao, F.; Zeng, J.; Li, M.; Shih, W. C. Label-Free, Zeptomole Cancer Biomarker Detection by Surface-Enhanced Fluorescence on Nanoporous Gold Disk Plasmonic Nanoparticles. *J. Biophotonics* **2015**, *8*, 855−863.

(8) Bhasikuttan, A. C.; Mohanty, J. Targeting G-Quadruplex Structures with Extrinsic Fluorogenic Dyes: Promising Fluorescence Sensors. *Chem. Commun.* **2015**, *51* (36), 7581−7597.

(9) Biffi, G.; Di Antonio, M.; Tannahill, D.; Balasubramanian, S. Visualization and Selective Chemical Targeting of Rna G-Quadruplex Structures in the Cytoplasm of Human Cells. *Nat. Chem.* **2014**, *6* (1), 75−80.

(10) Müller, S.; Kumari, S.; Rodriguez, R.; Balasubramanian, S. Small-Molecule-Mediated G-Quadruplex Isolation from Human Cells. *Nat. Chem.* **2010**, *2* (12), 1095−1098.

(11) Olejko, L.; Cywinski, P. J.; Bald, I. Ion-Selective Formation of a Guanine Quadruplex on DNA Origami Structures. *Angew. Chem., Int. Ed.* **2015**, *54* (2), 673−677.

(12) Koirala, D.; Dhakal, S.; Ashbridge, B.; Sannohe, Y.; Rodriguez, R.; Sugiyama, H.; Balasubramanian, S.; Mao, H. A Single-Molecule Platform for Investigation of Interactions between G-Quadruplexes and Small-Molecule Ligands. *Nat. Chem.* **2011**, *3* (10), 782−787.

(13) He, H. Z.; Chan, D. S.; Leung, C. H.; Ma, D. L. G-Quadruplexes for Luminescent Sensing and Logic Gates. *Nucleic Acids Res.* **2013**, *41* (8), 4345−4359.

(14) Bhasikuttan, A. C.; Mohanty, J.; Pal, H. Interaction of Malachite Green with Guanine-Rich Single-Stranded DNA: Preferential Binding to a G-Quadruplex. *Angew. Chem., Int. Ed.* **2007**, *46* (48), 9305−9307.

(15) Tarnok, I.; Czanik, P. A. L. Malachite Green - Reducing Enzyme in Mycobacteria. *Nature* **1959**, *183* (4660), 549−550.

(16) Norris, D. Reconstitution of Virus X-Saturated Potato Varieties with Malachite Green. *Nature* **1953**, *172* (4383), 816−816.

(17) Yang, M. C.; Fang, J. M.; Kuo, T. F.; Wang, D. M.; Huang, Y. L.; Liu, L. Y.; Chen, P. H.; Chang, T. H. Production of Antibodies for Selective Detection of Malachite Green and the Related Triphenylmethane Dyes in Fish and Fishpond Water. *J. Agric. Food Chem.* **2007**, *55* (22), 8851−8856.

(18) Guo, Z.; Gai, P.; Hao, T.; Duan, J.; Wang, S. Determination of Malachite Green Residues in Fish Using a Highly Sensitive Electrochemiluminescence Method Combined with Molecularly Imprinted Solid Phase Extraction. *J. Agric. Food Chem.* **2011**, *59* (10), 5257−5262.

(19) Srivastava, S.; Sinha, R.; Roy, D. Toxicological Effects of Malachite Green. *Aquat. Toxicol.* **2004**, *66* (3), 319−329.

(20) Stead, S. L.; Ashwin, H.; Johnston, B.; Dallas, A.; Kazakov, S. A.; Tarbin, J. A.; Sharman, M.; Kay, J.; Keely, B. J. An Rna-Aptamer-Based Assay for the Detection and Analysis of Malachite Green and Leucomalachite Green Residues in Fish Tissue. *Anal. Chem.* **2010**, *82* (7), 2652−2660.

(21) Patra, P. P.; Chikkaraddy, R.; Tripathi, R. P. N.; Dasgupta, A.; Kumar, G. V. P. Plasmofluidic Single-Molecule Surface-Enhanced Raman Scattering from Dynamic Assembly of Plasmonic Nanoparticles. *Nat. Commun.* **2014**, *5*, 4357.

(22) Liu, T.-Y.; Tsai, K.-T.; Wang, H.-H.; Chen, Y.; Chen, Y.-H.; Chao, Y.-C.; Chang, H.-H.; Lin, C.-H.; Wang, J.-K.; Wang, Y.-L. Functionalized Arrays of Raman-Enhancing Nanoparticles for Capture and Culture-Free Analysis of Bacteria in Human Blood. *Nat. Commun.* **2011**, *2*, 538.

(23) Kong, K. V.; Lam, Z.; Lau, W. K.; Leong, W. K.; Olivo, M. A Transition Metal Carbonyl Probe for Use in a Highly Specific and Sensitive Sers-Based Assay for Glucose. *J. Am. Chem. Soc.* **2013**, *135* (48), 18028−18031.

(24) Lang, X. Y.; Guan, P. F.; Zhang, L.; Fujita, T.; Chen, M. W. Characteristic Length and Temperature Dependence of Surface Enhanced Raman Scattering of Nanoporous Gold. *J. Phys. Chem. C* **2009**, *113* (25), 10956−10961.

(25) Zhang, L.; Chen, L.; Liu, H.; Hou, Y.; Hirata, A.; Fujita, T.; Chen, M. Effect of Residual Silver on Surface-Enhanced Raman Scattering of Dealloyed Nanoporous Gold. *J. Phys. Chem. C* **2011**, *115* (40), 19583−19587.

(26) Zhong, L. B.; Yin, J.; Zheng, Y. M.; Liu, Q.; Cheng, X. X.; Luo, F. H. Self-Assembly of Au Nanoparticles on Pmma Template as Flexible, Transparent, and Highly Active Sers Substrates. *Anal. Chem.* **2014**, *86* (13), 6262−6267.

(27) Fu, W. L.; Zhen, S. J.; Huang, C. Z. One-Pot Green Synthesis of Graphene Oxide/Gold Nanocomposites as Sers Substrates for Malachite Green Detection. *Analyst* **2013**, *138* (10), 3075−3081.

(28) Tan, E. Z.; Yin, P. G.; You, T. T.; Wang, H.; Guo, L. Three Dimensional Design of Large-Scale Tio(2) Nanorods Scaffold Decorated by Silver Nanoparticles as Sers Sensor for Ultrasensitive Malachite Green Detection. *ACS Appl. Mater. Interfaces* **2012**, *4* (7), 3432−3437.

(29) Hou, Y.; Zhang, L.; Chen, L. Y.; Liu, P.; Hirata, A.; Chen, M. W. Raman Characterization of Pseudocapacitive Behavior of Polypyrrole on Nanoporous Gold. *Phys. Chem. Chem. Phys.* **2014**, *16* (8), 3523−3528.

(30) Zhao, F.; Zeng, J.; Parvez Arnob, M. M.; Sun, P.; Qi, J.; Motwani, P.; Gheewala, M.; Li, C. H.; Paterson, A.; Strych, U.; Raja, B.; Willson, R. C.; Wolfe, J. C.; Lee, T. R.; Shih, W. C. Monolithic Npg Nanoparticles with Large Surface Area, Tunable Plasmonics, and High-Density Internal Hot-Spots. *Nanoscale* **2014**, *6* (14), 8199−8207.

(31) Arnob, M. M.; Zhao, F.; Zeng, J.; Santos, G. M.; Li, M.; Shih, W. C. Laser Rapid Thermal Annealing Enables Tunable Plasmonics in Nanoporous Gold Nanoparticles. *Nanoscale* **2014**, *6* (21), 12470−12475.

(32) Qi, J.; Motwani, P.; Gheewala, M.; Brennan, C.; Wolfe, J. C.; Shih, W. C. Surface-Enhanced Raman Spectroscopy with Monolithic Nanoporous Gold Disk Substrates. *Nanoscale* **2013**, *5* (10), 4105−4109.

(33) Zeng, J.; Zhao, F.; Li, M.; Li, C.-H.; Lee, T. R.; Shih, W.-C. Morphological Control and Plasmonic Tuning of Nanoporous Gold Disks by Surface Modifications. *J. Mater. Chem. C* **2015**, *3* (2), 247−252.

(34) Zeng, J.; Zhao, F.; Qi, J.; Li, Y.; Li, C.-H.; Yao, Y.; Lee, T. R.; Shih, W.-C. Internal and External Morphology-Dependent Plasmonic Resonance in Monolithic Nanoporous Gold Nanoparticles. *RSC Adv.* **2014**, *4* (69), 36682−36688.

(35) Li, M.; Du, Y.; Zhao, F.; Zeng, J.; Mohan, C.; Shih, W.-C. Reagent-and Separation-Free Measurements of Urine Creatinine Concentration Using Stamping Surface Enhanced Raman Scattering (S-Sers). *Biomed. Opt. Express* **2015**, *6* (3), 849−858.

(36) Lin, S.; Zhu, W.; Jin, Y.; Crozier, K. B. Surface-Enhanced Raman Scattering with Ag Nanoparticles Optically Trapped by a Photonic Crystal Cavity. *Nano Lett.* **2013**, *13* (2), 559−563.

DOI: 10.1021/acsami.6b09767
ACS Appl. Mater. Interfaces 2016, 8, 29968−29976

(37) Zhang, L.; Lang, X.; Hirata, A.; Chen, M. Wrinkled Nanoporous Gold Films with Ultrahigh Surface-Enhanced Raman Scattering Enhancement. *ACS Nano* **2011**, *5* (6), 4407−4413.
(38) Mohanty, J.; Barooah, N.; Dhamodharan, V.; Harikrishna, S.; Pradeepkumar, P. I.; Bhasikuttan, A. C. Thioflavin T as an Efficient Inducer and Selective Fluorescent Sensor for the Human Telomeric G-Quadruplex DNA. *J. Am. Chem. Soc.* **2013**, *135* (1), 367−376.
(39) Das, J.; Ivanov, I.; Montermini, L.; Rak, J.; Sargent, E. H.; Kelley, S. O. An Electrochemical Clamp Assay for Direct, Rapid Analysis of Circulating Nucleic Acids in Serum. *Nat. Chem.* **2015**, *7* (7), 569−575.
(40) Zhang, Y.; Yu, W.; Pei, L.; Lai, K.; Rasco, B. A.; Huang, Y. Rapid Analysis of Malachite Green and Leucomalachite Green in Fish Muscles with Surface-Enhanced Resonance Raman Scattering. *Food Chem.* **2015**, *169*, 80−84.
(41) Sudheendran, N.; Qi, J.; Young, E. D.; Lazar, A. J.; Lev, D. C.; Pollock, R. E.; Larin, K. V.; Shih, W.-C. Line-Scan Raman Microscopy Complements Optical Coherence Tomography for Tumor Boundary Detection. *Laser Phys. Lett.* **2014**, *11* (10), 105602.
(42) Liu, C.-H.; Qi, J.; Lu, J.; Wang, S.; Wu, C.; Shih, W.-C.; Larin, K. V. Improvement of Tissue Analysis and Classification Using Optical Coherence Tomography Combined with Raman Spectroscopy. *J. Innovative Opt. Health Sci.* **2015**, *08* (04), 1550006.
(43) Vilar, M. R.; Botelho do Rego, A. M.; Ferraria, A. M.; Jugnet, Y.; Nogues, C.; Peled, D.; Naaman, R. Interaction of Self-Assembled Monolayers of DNA with Electrons: Hreels and Xps Studies. *J. Phys. Chem. B* **2008**, *112* (23), 6957−6964.
(44) Le Ru, E. C.; Etchegoin, P. G. Single-Molecule Surface-Enhanced Raman Spectroscopy. *Annu. Rev. Phys. Chem.* **2012**, *63*, 65−87.
(45) Pedireddy, S.; Lee, H. K.; Tjiu, W. W.; Phang, I. Y.; Tan, H. R.; Chua, S. Q.; Troadec, C.; Ling, X. Y. One-Step Synthesis of Zero-Dimensional Hollow Nanoporous Gold Nanoparticles with Enhanced Methanol Electrooxidation Performance. *Nat. Commun.* **2014**, *5*, 4947.
(46) Kreig, A.; Calvert, J.; Sanoica, J.; Cullum, E.; Tipanna, R.; Myong, S. G-Quadruplex Formation in Double Strand DNA Probed by Nmm and Cv Fluorescence. *Nucleic Acids Res.* **2015**, *43* (16), 7961−7970.
(47) Qiu, S.; Miao, M.; Wang, T.; Lin, Z.; Guo, L.; Qiu, B.; Chen, G. A Fluorescent Probe for Detection of Histidine in Cellular Homogenate and Ovalbumin Based on the Strategy of Click Chemistry. *Biosens. Bioelectron.* **2013**, *42*, 332−336.
(48) Zhu, S.; Zhang, X.; Cui, J.; Shi, Y. E.; Jiang, X.; Liu, Z.; Zhan, J. Silver Nanoplate-Decorated Copper Wire for the on-Site Micro-extraction and Detection of Perchlorate Using a Portable Raman Spectrometer. *Analyst* **2015**, *140* (8), 2815−2822.
(49) Lin, K.; Wang, J.; Zheng, W.; Ho, K. Y.; Teh, M.; Yeoh, K. G.; Huang, Z. Rapid Fiber-Optic Raman Spectroscopy for Real-Time in Vivo Detection of Gastric Intestinal Metaplasia During Clinical Gastroscopy. *Cancer Prev. Res.* **2016**, *9* (6), 476−483.
(50) Hartley, J. S.; Juodkazis, S.; Stoddart, P. R. Optical Fibers for Miniaturized Surface-Enhanced Raman-Scattering Probes. *Appl. Opt.* **2013**, *52* (34), 8388−8393.

DOI: 10.1021/acsami.6b09767
ACS Appl. Mater. Interfaces 2016, 8, 29968−29976